

REVISED VERSION November 22, 2018

The evolution of the galactic morphological types in clusters

Giovanni Fasano,¹ Bianca M. Poggianti,¹ Warrick J. Couch,² Daniela Bettoni,¹ Per Kjærgaard,³ Mariano Moles⁴

1) Osservatorio Astronomico di Padova, vicolo dell’Osservatorio 5, 35122 Padova, Italy.

2) School of Physics, University of New South Wales, Sydney 2052, Australia.

3) Astronomical Observatory of Copenhagen University, Juliane Maries Vej 30, 2100 Copenhagen, DK

4) Instituto de Matematicas y Fisica Fundamental, CSIC, C/ Serrano 123, 28006 Madrid, Spain.

ABSTRACT

The morphological types of galaxies in nine clusters in the redshift range $0.1 \lesssim z \lesssim 0.25$ are derived from very good seeing images taken at the NOT and the La Silla–Danish telescopes, with all galaxies at $M_V < -20$ and within the central $\sim 1 \text{ Mpc}^2$ area being classified. With the purpose of investigating the evolution of the fraction of different morphological types with redshift, we compare our results with the morphological content of nine distant clusters studied by the MORPHS group (Dressler et al. 1997), five clusters observed with *HST-WFPC2* at redshift $z = 0.2 - 0.3$ (Couch et al. 1998), and Dressler’s (1980) large sample of nearby clusters. After having checked the reliability of our morphological classification both in an absolute sense and relative to the MORPHS scheme (Smail et al. 1997), we analyze the relative occurrence of elliptical, S0 and spiral galaxies as a function of the cluster properties and redshift. We find a large intrinsic scatter in the S0/E ratio, mostly related to the cluster morphology. In particular, in our cluster sample, clusters with a high concentration of ellipticals display a low S0/E ratio and, vice-versa, low concentration clusters have a high S0/E. At the same time, the trend of the morphological fractions (%Es, %S0s, %Sp) and of the S0/E and S0/Sp ratios with redshift clearly points to a morphological evolution: as the redshift decreases, the S0 population tends to grow at the expense of the spiral population, whereas the frequency of Es remains almost constant. We also analyze the morphology-density (MD) relation in our clusters and find that – similarly to higher redshift clusters – a good MD relation exists in the high-concentration clusters, while it is absent in the less concentrated clusters. Finally, the comparison of the MD relation in our clusters with that of the D97 sample suggests that the transformation of spirals into S0 galaxies becomes more efficient with decreasing local density.

Subject headings: galaxies: clusters – galaxies: evolution – galaxies: structure

Received _____; accepted _____

1. Introduction

When Butcher & Oemler (1978, 1984) discovered an excess of galaxies bluer than the elliptical sequence in clusters at $z \geq 0.2$, nothing was known about the galactic morphologies at such large distances. The first evidence of the disky/spiral nature of the Butcher-Oemler galaxies came from high-resolution ground-based imagery which also found several cases of galaxies with disturbed morphologies and/or close neighbors (Thompson 1986, 1988, Lavery & Henry 1988, 1994, Lavery, Pierce & McClure 1992).

Over the past five years, thanks to the high spatial resolution imaging achieved with the *Hubble Space Telescope* (*HST*), it has been established that the morphological properties of galaxies in rich clusters at intermediate redshift differ dramatically from those in nearby clusters. The most obvious difference is the overabundance of spirals in the cluster cores at $z = 0.3 - 0.5$ (Couch et al. 1994, 1998, Dressler et al. 1994, Wirth et al. 1994, Dressler et al. 1997 [D97, MORPHS collaboration], Oemler et al. 1997, Smail et al. 1997 [S97, MORPHS]). The spiral population in the distant clusters consist of the great majority of the blue galaxies responsible for the Butcher-Oemler effect, as well as a sizeable fraction of the red population (Dressler et al. 1999 [MORPHS], Poggianti et al. 1999 [MORPHS]). A considerable proportion of these spirals have disturbed morphologies, in some cases quite clearly as the result of an ongoing merger/interaction while in others possibly connected to some other dynamical mechanism (e.g. interaction with the hot intracluster medium or the cluster tidal field, Moore et al. 1996, 1998, Abadi et al. 1999).

The second major piece of evidence for morphological evolution in clusters was uncovered only from post-refurbishment data: Coupled to the increase in the spiral fraction, the S0 galaxies at intermediate redshifts are proportionately (x2–3) less abundant than in nearby clusters, while the fraction of ellipticals is already as large or larger (D97, S97). This result strongly suggests that a large number of the cluster spirals observed at $z \sim 0.4$ have evolved into the S0's that dominate the cores of rich clusters today (D97, Couch et al. 1998, van Dokkum et al. 1998, but see Andreon 1998 for a different view). Thus the disk galaxy populations appear to be greatly affected by the cluster environment, while the ellipticals in dense regions seem to have changed little since $z \sim 0.5$ as far as both their abundance and their stellar populations are concerned (van Dokkum & Franx 1996, Andreon, Davoust & Heim 1997, D97, Ellis et al. 1997 (MORPHS), Kelson et al. 1997, S97, Barger et al. 1998 (MORPHS), van Dokkum et al. 1998, Kelson et al. 1999). Morphological studies at redshift greater than 0.6 have been limited to three clusters so far, pointing to a low fraction of early-type galaxies in two clusters at $z \sim 0.8$ (Lubin et al. 1998, van Dokkum et al. 2000), a high early-type galaxy fraction in a cluster at $z=0.9$ (Lubin et al. 1998) and a surprisingly high rate of mergers in a cluster at $z=0.83$ (van Dokkum et al. 1999).

Further proof of the changes occurring in clusters is the observed evolution of the morphology-density (MD) relation – the correlation between galaxy morphology and local projected density of galaxies that Dressler (1980a, D80a) found *in all types of clusters* at low redshift, whereby the elliptical fraction increases and the spiral fraction decreases with increasing local galaxy density. An MD relation qualitatively similar to that found by D80a was discovered by D97 to be present *in regular clusters and absent in irregular ones at $z \sim 0.5$* . Interestingly, the incidence of ellipticals is already very high in all the distant clusters regardless of their dynamical status, therefore the formation of the ellipticals must occur independently of and before cluster virialization (D97).

Overall, the available data seem to require a strong morphological evolution in clusters between $z = 0.4$ and $z = 0$. Still, it is worth keeping in mind that these conclusions, although grounded on high-quality data obtained with a monumental observational effort, are based on a “small” sample of distant

clusters and on the comparison of a limited redshift range around $z \sim 0.4$ with the present-day cluster populations (Dressler 1980b, D80b). Clearly the $z \sim 0.1 - 0.2$ regime - which up until now has remained largely unexplored - is crucial for a better understanding of the progression of galaxy evolution in dense environments. At these moderate redshifts, performing an analysis comparable to that of the MORPHS requires either ground-based CCD imaging taken over quite a large field under excellent seeing conditions, or a time-consuming mosaic coverage with *HST*.

The goal of this paper is to begin to fill in the observational gap between the distant clusters observed with *HST* and the nearby clusters, and hence trace, for the first time, the evolution of the morphological mix at a look-back time of 2 – 4 Gyr. In addition, by enlarging the sample of clusters whose galactic morphologies have been studied in detail, we hope to shed some light on the dependence of the observed evolutionary trends on the cluster properties. We present ground-based, good-seeing images of the central regions of 9 clusters at $z = 0.09 - 0.25$ (§2) and we perform a detailed morphological analysis of the galaxies in these clusters (§3). We study the relative occurrence of ellipticals, S0's and spirals as a function of the cluster properties and we compare them with similar studies at lower and higher redshift (§4). Finally, we examine the morphology-density relation of the total sample and of the high- and low-concentration clusters separately (§5) and we present our conclusions in §6. Throughout this paper we use $H_0 = 50 \text{ km sec}^{-1} \text{ Mpc}^{-1}$ and $q_0 = 0.5$.

2. Observations and sample selection

The data presented here we taken as part of a long term project, involving four of us (GF,DB,PK,MM), aimed at analysing the scaling relations of early-type galaxies in 25 clusters spanning the redshift range 0.03 – 0.25 (Fasano et al. 2000). Only Abell clusters having Bautz and Morgan (1970) types II or larger, Rood and Sastry (1971) types C or F, and galactic latitude $|b| > 40^\circ$ were included in the original sample. Moreover, very poor clusters (Abell richness class = 0) were excluded from the selection.

The observations, taken in two or three bands (B , V , Gunn r), were collected at the NOT (STAN-CAM or ALFOSC) and 1.5 Danish (DFOSC) telescopes during four different observing runs from May 1995 to Feb 1997. A log of the observations pertinent to the clusters discussed in this paper, together with the main properties of the CCDs used, are presented in Table 1. The seeing at the NOT telescope ranged from 0.5 to 0.82 arcsec, except during run (4) when it was 1.1 arcsec; at the 1.5 Danish telescope (run 3) the seeing was ~ 1.5 arcsec. However, the rest-frame resolution in kpc does not vary much within the sample (see Table 2). Several standard star fields (Landolt 1992) were observed during each night in the three bands in order to set the proper photometric calibrations as a function of the zenith distance and of the $B - G_r$ (or $V - G_r$) colors. Bias subtraction and flat-fielding, together with the removal of bad columns and cosmic ray events,

TABLE 1

| Run | Date | Instrument | Pixelsize (arcseconds) | Field (pixels) | gain | r.o.n. |
|-----|----------|------------|---------------------------|-------------------|------|--------|
| 1 | 1995 May | STAN-CAM | 0.176 | 1024 ² | 1.69 | 6.36 |
| 2 | 1995 Jun | STAN-CAM | 0.176 | 1024 ² | 1.69 | 6.36 |
| 3 | 1997 Jan | DFOSC | 0.420 | 2052 ² | 1.31 | 4.90 |
| 4 | 1997 Feb | ALFOSC | 0.187 | 2048 ² | 1.02 | 5.60 |

were performed using the *CCDPROC* tool in IRAF. A more detailed description of the observations and data reduction procedures can be found in Fasano et al. (2000).

To be consistent with previous morphological studies (D97), we should only consider clusters for which at least the central 1 Mpc^2 has been imaged. Due to the limited angular size of our CCD frames, we have excluded from the present sample those clusters with $z < 0.09$, for which the coverage turned out to be inadequate. Moreover, since our observations were not conceived in order to satisfy the above mentioned criterion, even for clusters with $z > 0.1$ the sampled area is sometimes less than 1 Mpc^2 and it often turns out to be shifted with respect to the geometrical center of the cluster. Hence, among the 25 clusters observed as part of the scaling-relation program, we have selected 9 clusters in the redshift range $0.1 \lesssim z \lesssim 0.25$ for which an acceptable coverage of the central region has been secured.

The basic information concerning the selected clusters and the parameters relevant for our analysis are reported in Table 2. For two clusters, A2658 and A1878, the available frames cover about half of the requested area: in the following we will explain how we have tried to account for the partial coverage. For Abell 2192 we list two different entries in Table 2: the first one (run 1) refers to four contiguous Gunn *r* images covering a quite large area, the second one (run 2) relates to a smaller part of the cluster, for which (*B-r*) colors of galaxies are available, thus allowing a more accurate photometric calibration. When comparing with the other clusters, we will refer to the large area image of A2192, while we will make use of the smaller area to assess how strongly the different coverage can affect the results.

3. Galaxy catalogs and morphological classification

Catalogs of galaxies for each frame have been obtained using SExtractor (Bertin and Arnouts 1996). The galaxy magnitudes have been corrected for a well known bias affecting SExtractor magnitudes of galaxies having an $r^{1/4}$ profile (Franceschini et al. 1998).

As in D97, the analysis of the morphological types has been done for galaxies down to a visual absolute magnitude $M_V \sim -20.0$. The corresponding *r*-band magnitude limits were derived using standard Gunn-*r* and Cousins/Johnson (*V*) filter transmission, first adopting the conversion between Gunn-*r* and Cousins *R* given by Jorgensen (1994) and then applying the K-corrections of an intermediate energy distribution

TABLE 2

| Cluster | z | RA (J2000) | DEC (J2000) | E(B-V) | Run | area Mpc^2 | seeing arcsec | seeing kpc | M_{lim} (Gunn r) |
|----------|-------|---|----------------|--------|-----|------------------------|------------------|---------------|-----------------------|
| A3330 | 0.091 | 05 ^h 14 ^m 47 ^s | -49° 04' 19" | 0.00 | 3 | 1.0 | 1.53 | 3.46 | 18.36 |
| A389 | 0.116 | 02 ^h 51 ^m 31 ^s | -24° 56' 05" | 0.00 | 3 | 1.2 | 1.45 | 4.04 | 18.85 |
| A951 | 0.143 | 10 ^h 13 ^m 55 ^s | +34° 43' 06" | 0.01 | 4 | 1.0 | 1.10 | 3.65 | 19.34 |
| A2658 | 0.185 | 23 ^h 44 ^m 59 ^s | -12° 18' 20" | 0.10 | 2 | 0.4 | 0.70 | 2.78 | 20.46 |
| A2192(l) | 0.187 | 16 ^h 26 ^m 37 ^s | +42° 40' 20" | 0.01 | 1 | 1.8 | 0.55 | 2.22 | 20.21 |
| A2192(s) | 0.187 | 16 ^h 26 ^m 37 ^s | +42° 40' 20" | 0.01 | 2 | 0.4 | 0.82 | 3.31 | 20.21 |
| A1643 | 0.198 | 12 ^h 55 ^m 54 ^s | +44° 04' 46" | 0.00 | 1 | 0.9 | 0.50 | 2.10 | 20.33 |
| A2111 | 0.229 | 15 ^h 39 ^m 38 ^s | +34° 24' 21" | 0.06 | 1 | 0.9 | 0.70 | 3.22 | 20.80 |
| A1952 | 0.248 | 14 ^h 41 ^m 04 ^s | +28° 38' 12" | 0.00 | 2 | 1.2 | 0.60 | 2.93 | 20.92 |
| A1878 | 0.254 | 14 ^h 12 ^m 49 ^s | +29° 12' 59" | 0.00 | 1 | 0.6 | 0.50 | 2.47 | 20.92 |

(Sab) for $H_0 = 50 \text{ km sec}^{-1} \text{ Mpc}^{-1}$ and $q_0 = 0.5$. Examples of K-corrections for various galactic types can be found in Poggianti (1997). The magnitude limits were corrected for the foreground Galactic extinction (see Table 2) according to the standard Galactic extinction law (Mathis 1990).

Column 8 of Table 2 reports the seeing in arcseconds, whereas column 9 shows the rest-frame resolution that ranges between 2 and 4 kpc. Even though the seeing quality of our imagery was often excellent, the spatial resolution is poorer than that secured by the *HST* imaging of the clusters in D97 ($\sim 0.7 \text{ kpc}$ at $z \sim 0.5$), making the merely visual classification less reliable with respect to that given by the MORPHS. In order to improve the morphological type estimates we have produced luminosity and geometrical (ellipticity and position angle) profiles of all selected galaxies using the automatic surface photometry tool *GASHOT* (Pignatelli and Fasano 1999). In this way, in addition to the appearance of the galaxies on the images and to the surface and isophotal plots, we took advantage of the typical indications coming from the morphological profiles. For instance, S0 galaxies, even if poorly resolved, are usually characterized by increasing ellipticity profiles (indicating an extended disk superimposed upon an inner, round bulge), composite luminosity profiles (with $r^{1/4}$ inner part and exponential outer part) and almost constant position angle profiles in the outer part (disk). In contrast, constant (or even decreasing) ellipticity profiles and outer isophotal twisting (together with ‘pure’ $r^{1/4}$ luminosity profile) are highly suggestive of an elliptical morphology. An exponential luminosity profile, with almost constant (or fluctuating) position angle and ellipticity profiles are good hints of spiral morphology. A break-down in ellipticity, coupled with a sharp (and large) change of position angle, usually indicates the presence of a bar, thus suggesting a spiral (or S0) classification. Clearly, the above indications cannot be considered as unfailing rules, but certainly they contributed to make the classifications more robust. Table 3 (available on CD-ROM form) reports the positions and the morphological classifications of all galaxies in our sample.

The morphological classification of the selected galaxies was done by GF on the *r*-band images relying on both the visual appearance and the profiles. Galaxies whose broad classification (E/S0/Sp) was judged uncertain have been recorded with a question mark (eg: E?, S0?, Sp?) in Table 3. The transition objects (E/S0, S0/E, S0/a, Sa/0) have been ‘arbitrarily’ assigned to some broad class (E/S0/Sp) on the basis of the experience and of the opinion of the classifier (GF). However, the relative number of galaxies with uncertain and/or transition morphology turns out to add a negligible contribution to the errorbars of the morphological frequencies which are dominated by the Poissonian uncertainties.

It is obviously crucial for our purposes to assess the reliability of our classification scheme both in an absolute sense and relative to the MORPHS scheme. To this end we have devised four different ‘blind’ tests. The absolute accuracy of our classification has been checked in two ways:

- a) Using the *MKOBJECTS* tool in IRAF, we have produced a set of ‘toy’ galaxies with different bulge/disk luminosity and size ratios and varying inclination, trying to reproduce E, S0, Sa and Sbc galaxies according to the typical ratios given by Simien and de Vaucouleurs (1986). The proper values of noise, seeing, pixel size and redshift have been used in the simulations to mimic, at best, the observing conditions of the cluster A2111 at $z=0.23$ which represents an average case for its seeing and rest-frame resolution (0.7 arcsec, 3.22 kpc). The toy galaxies have been then classified using the same tools and the same classification scheme used for real galaxies.
- b) The nearby galaxy imaging collection of Frei et al. (1996) has been used to produce redshifted versions (with the $\sim (1+z)^4$ surface brightness dimming taken into account) of 34 galaxies of different morphological types, including all the galaxies listed by Frei et al. to have types E to Sa ($T=-5$ to 1) and eight later-type galaxies ($T=2$ to 6). In this way we intended to verify the capacity to discriminate between

ellipticals, S0s and early-type spirals and to recognize later-type galaxies, the latter being an easier task than the former. Again the proper values of the observing parameters have been used to mimic our A2111 images and the resulting galaxies have been classified following the procedure and the rules used for our cluster galaxies.

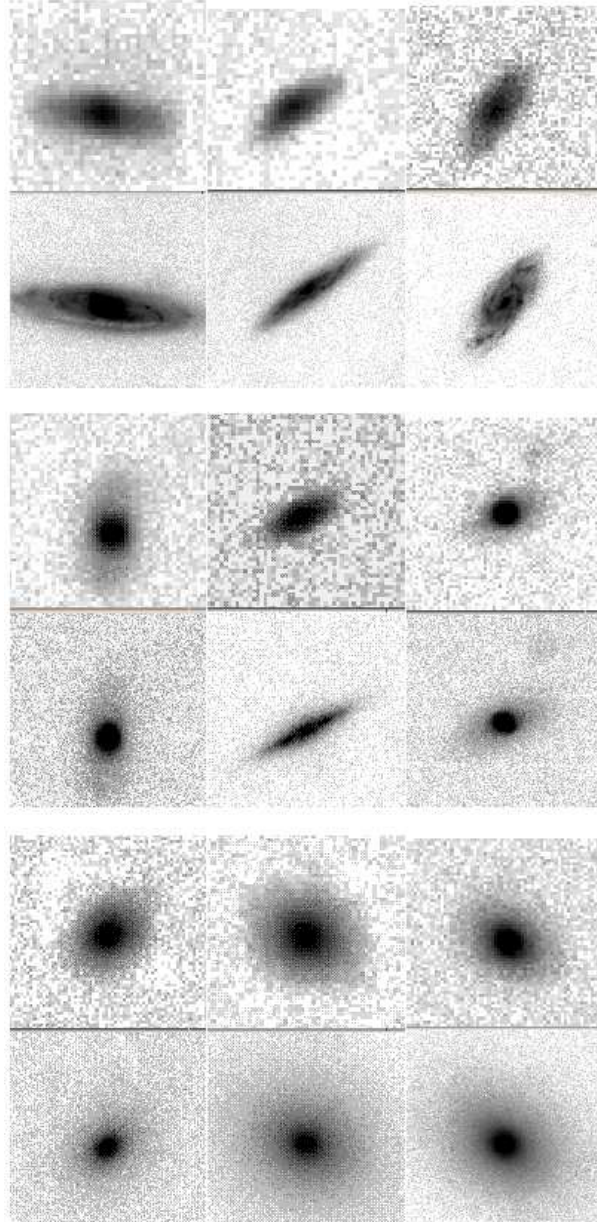


Fig. 1.(to be viewed in landscape) – Examples of Frei's nearby galaxy images (lower row of each set) compared with the corresponding redshifted versions (upper row of each set). Three galaxies for each broad morphological type (E:S0:Sp) are presented. From bottom to top: the elliptical galaxies NGC 4365, NGC 4472 and NGC 4636; the S0 galaxies NGC 3166, NGC 4710 and NGC 4754; the spiral galaxies NGC 3623, NGC 3877 and NGC 6118.

In Figure 1 three examples of Frei’s nearby galaxy images for each broad class (E:S0:Sp) are shown, together with the corresponding redshifted versions.

The main goal of these tests is to determine whether the quality of our images is sufficient to recognize, at the cluster redshifts, the salient features of the galactic morphologies, enabling us to broadly classify galaxies into ellipticals (E,E?,E/S0), S0s (S0,S0?,S0/E,S0/a) and spirals (Sa/0 and later) *as we would do for nearby galaxies*. These tests show that in the great majority of cases (89% in test [a] and 73% in test [b]) the broad morphological types (E, S0 and spirals) assigned by GF at $z=0$ are also recovered at $z \sim 0.23$ with no systematic shift among the types. The only exception is represented by those galaxies from Frei’s catalog that were classified as S0/a at $z=0$. In fact, half of them enter the “spiral class” as early spirals when viewed at $z=0.23$, while in our classification the S0/a galaxies belongs to the S0 class. Excluding these S0/a galaxies, low-z ellipticals, S0s and spirals were recovered at $z=0.23$ in the 92% (11/12), 71% (5/7) and 100% (8/8) of the cases, respectively. Test a) shows that, regardless of the redshift, the seeing conditions, etc, S0 galaxies viewed face-on are classified ellipticals, while the inclination of S0 and Sa galaxies influences the assignment to one class or the other as edge-on S0s are easily mistaken for Sa’s, while Sa’s at small inclinations are classified S0’s.

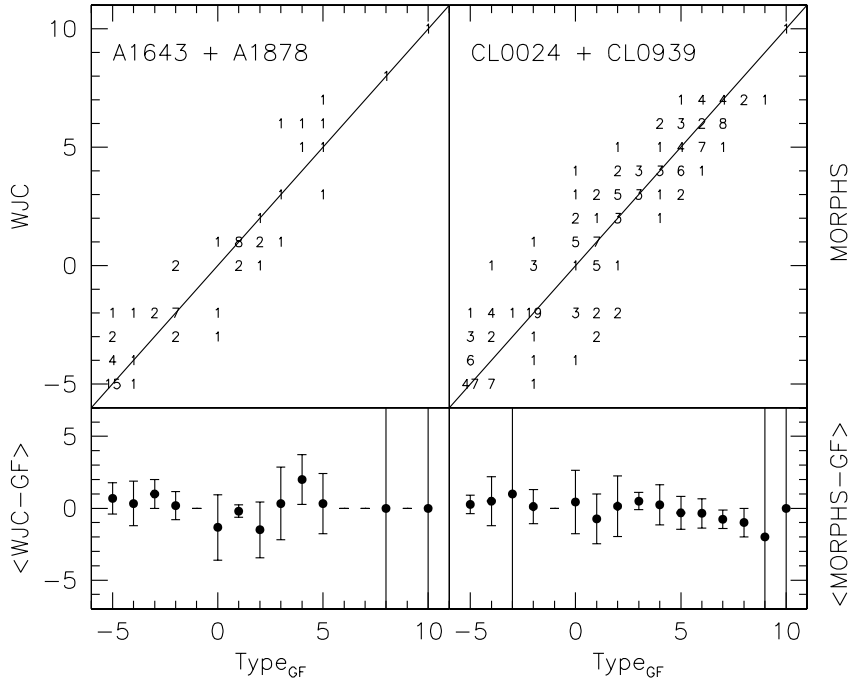


Fig. 2. – *Upper-left panel:* comparison between the de Vaucouleurs T types assigned by GF and WJC in their classifications of 67 galaxies from the groundbased (NOT) imaging of the clusters Abell 1643 and Abell 1878. The number of galaxies in each bin of the GF versus WJC plane is indicated. *Upper-right panel:* comparison between the de Vaucouleurs T types assigned by GF and the MORPHS in their *HST*-based classifications of the clusters CL 0024+16 and CL 0939+47. *Lower panels:* average differences between the external and the GF types versus the GF classifications. Error bars illustrate the statistical variances.

In the tests described above, our types are compared with morphological classifications which are

considered correct *a priori*, since they refer to toy or nearby galaxies. However, in order to be able to compare our results with higher redshift clusters, besides an absolute check, we need to test the consistency between our classifications and those of the MORPHS group. This has been done in two ways:

c) GF undertook independent visual classifications of galaxies in the MORPHS *HST* images of the clusters CL 0024+16 and CL 0939+47.

d) WJC (one of the classifiers of the MORPHS collaboration) has provided independent visual classifications of 67 galaxies in two clusters of the present sample (Abell 1643 and Abell 1878).

The results of tests c) and d) are summarized in Figure 2. At first sight the agreement between GF and the external classifiers seems to be quite good. However, after counting the total number of galaxies which, according to the different classifiers, fall in the different broad morphological types (E/S0/Sp), it was found that GF had classified a smaller number of galaxies as S0 in comparison to WJC and the MORPHS (57 versus 73). Twelve of these galaxies GF had classified as ellipticals, while the remaining 4 had been classified as spirals.

We stress that these differences are actually not statistically significant as far as the counts are concerned. In the worst case – the S0 galaxies – the Poissonian uncertainties are such that the difference in numbers between GF and the other classifiers (57 cf. 73) represents only a 1.5σ margin. Nevertheless, to be conservative, we have assumed the above difference in assignment between the classifiers to be systematic. In section 5, where an overall discussion of all available data will be presented, in order to consistently compare our data with those from the MORPHS sample, we will introduce a statistical correction to account for these differences in the morphological classification.

An indirect, fully independent confirmation of the correctness of our morphological classifications may be obtained by looking at the ellipticity distribution of elliptical and S0 galaxies in our clusters. These distributions are shown in Figure 3, together with the ellipticity distribution of E galaxies derived by Fasano and Vio (1991) for a large sample of local objects (smooth solid line). The agreement with the corresponding distribution from our elliptical galaxy sample is fairly good, supporting the assumption that we are sampling the same population. Moreover, our E and S0 ellipticity distributions are very similar to the corresponding ones shown in S97 and D97 for the MORPHS dataset, the Coma cluster (Andreon et al. 1996) and the nearby cluster sample of D80b. It is worth noting that the lack of round objects in the ellipticity distribution of S0 galaxies confirms the previously mentioned bias in the classification of face-on S0s (see test [a]). This kind of misclassification, however, has been shown to be almost unavoidable, even for nearby galaxies (Capaccioli et al. 1991).

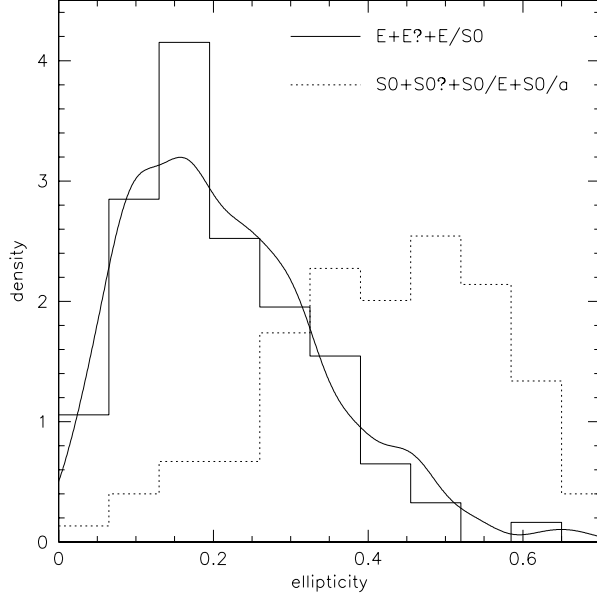


Fig. 3. Ellipticity distributions of elliptical and S0 galaxies in our clusters. The smooth solid line represents the ellipticity distribution of Es derived by Fasano and Vio (1991) for a large sample of local objects.

4. Results and comparison with other samples

In Table 4 we list, for each cluster, the observed numbers of Es, S0s and spirals and the observed S0/E ratio, together with the Poissonian error. The clusters appear to be grouped in two different families, according to their S0/E ratios: a low S0/E family (4 clusters) with $S0/E \sim 0.5$, and a high S0/E family (5 clusters) with $S0/E \gtrsim 1.1$. We note that if we apply to our counts a statistical correction to compensate for the excess of Es and the lack of S0s we have found in our classifications with respect to the MORPHS (see §3), the S0/E ratios of the above mentioned families both shift upwards, but the dichotomy remains (see Figure 10a). We have investigated whether this S0/E dichotomy could be driven by the small

TABLE 4: MORPHOLOGICAL COUNTS OF OUR CLUSTERS

| Cluster | z | E | S0 | Sp | S0/E |
|-------------|-------|----|----|----|-----------------|
| 1) A3330 | 0.091 | 18 | 18 | 11 | 1.00 ± 0.33 |
| 2) A 389 | 0.116 | 17 | 18 | 3 | 1.06 ± 0.36 |
| 3) A951 | 0.143 | 10 | 12 | 2 | 1.20 ± 0.50 |
| 4) A2658 | 0.185 | 11 | 6 | 3 | 0.54 ± 0.29 |
| 5) A2192(l) | 0.187 | 17 | 18 | 14 | 1.06 ± 0.36 |
| 5) A2192(s) | 0.187 | 9 | 12 | 5 | 1.33 ± 0.59 |
| 6) A1643 | 0.198 | 15 | 17 | 15 | 1.13 ± 0.40 |
| 7) A2111 | 0.229 | 34 | 17 | 16 | 0.50 ± 0.14 |
| 8) A1952 | 0.248 | 25 | 14 | 14 | 0.56 ± 0.20 |
| 9) A1878 | 0.254 | 15 | 8 | 15 | 0.53 ± 0.23 |

cluster-to-cluster variations in the rest-frame characteristics of the images, but the observed S0/E ratio is found to be uncorrelated with the resolution and with the area surveyed as shown in Fig. 4a,b. ¹ Hence, the S0/E dichotomy seems to reflect an intrinsic difference in the relative proportions of these types of galaxies in the two subsets of clusters.

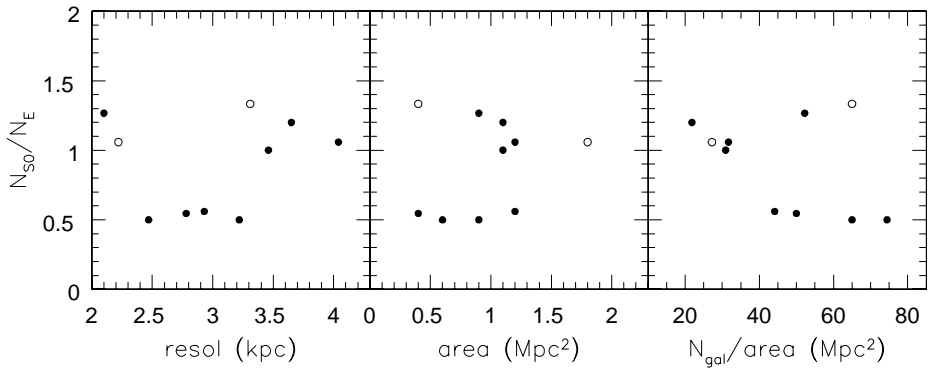


Fig. 4. The S0/E ratio versus the rest-frame resolution (in kpc), the area (in Mpc^2) and the mean galaxy density (in numbers of galaxies per Mpc^2). The *open* circles refer to A2192, where both the smallest area (0.4 Mpc^2) and the largest area (1.8 Mpc^2) values are plotted. Errorbars are not displayed for the sake of clarity and can be found in Table 4.

The low S0/E and the high S0/E clusters are at $z \geq 0.19$ and $z \leq 0.2$, respectively, but this step-like behaviour of the S0/E ratio at $z \sim 0.2$ is unlikely to be an abrupt evolutionary effect: rather, it could be related to different characteristics of the two families of clusters. Searching for correlations between the S0/E ratio and the global cluster properties, we have found no relation with the mean projected galaxy density (Fig. 4c). *The only structural difference between the low-S0/E and the high-S0/E clusters seems to be the presence/absence of a high concentration of elliptical galaxies in a region that is identified as the cluster centre.* This effect, visible even for individual clusters, is evident in Figure 5, where the centered 2^2 maps of the low-S0/E and high-S0/E clusters are superimposed separately on a rest-frame absolute scale.

¹The sensitivity of the S0/E ratio to the rest-frame area surveyed, was tested using A2192, which has large coverage. This showed only a modest effect (see also Table 2).

²In the following the cluster centers are defined, for each cluster, by the median coordinates of all galaxies. However, the results turn out to be very similar if a different definition of the center is adopted (i.e mean rather than median coordinates and/or elliptical rather than whole population).

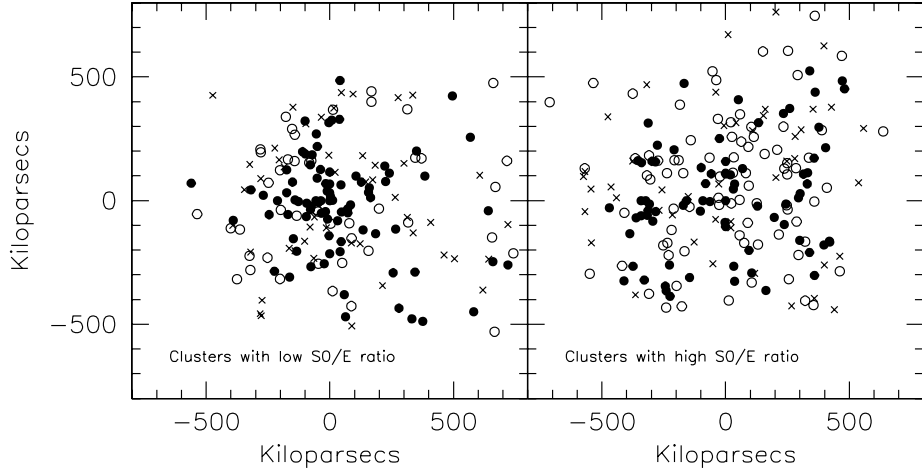


Fig. 5. Overlapping of the centered maps of the low-S0/E and high-S0/E clusters. Filled dots, open dots and crosses refer to ellipticals, S0s and spirals, respectively.

A more quantitative illustration of the difference in the galaxy spatial distribution between the low-S0/E and the high-S0/E clusters is given in Fig. 6 using the Kolmogorov–Smirnov (KS) test. The cumulative radial distribution of the ellipticals in the low-S0/E clusters is significantly steeper (i.e. more concentrated) than that of the high S0/E clusters. The two S0 distributions are practically indistinguishable and those of the spirals do not differ significantly, while the two total distributions of all types of galaxies are dominated by the ellipticals and are statistically different.

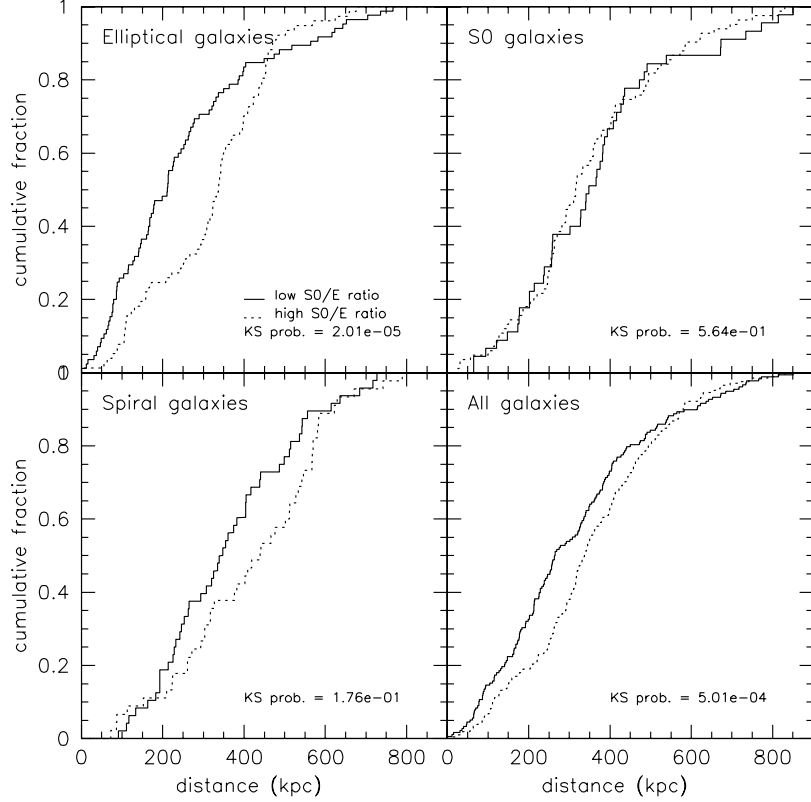


Fig. 6. Kolmogorov–Smirnov test applied to the overlapped radial distributions (see Figure 5) of galaxies of different types for low-S0/E (full lines) and high-S0/E (dotted lines) clusters.

It is worth stressing that, both the ‘first sight’ impression from Figure 5 and the ‘objective’ test in Figure 6 might actually be biased by the differences in the rest-frame sampled areas among the clusters, as well as by the slight off-centering of the CCD frames with respect to the cluster centers and by the irregular shape of the area surveyed. In an attempt to overcome this problem, we present in Figure 7 a different representation of the cumulative radial distributions. In this figure each line represents a different cluster (the numbers at the end of each line identify the clusters according to the ranking in Table 4) and the distributions are not normalized to the total number of galaxies. Moreover, in order to correct for incompleteness due to the irregular shape of the area surveyed, the cumulative numbers N_{CC} in Figure 7 are obtained by adding, for each new galaxy at increasing distance r , the quantity $1/C(r)$, where $C(r)$ is a completeness factor expressing the fraction of the circular area πr^2 which is actually included in the area surveyed. These corrections turn out to be small and never exceed 10%. Even though not quantifiable by statistical tests like a KS, in Figure 7 the difference in the concentration of the elliptical population between low-S0/E (full lines) and high-S0/E (dashed lines) clusters stands out, with the low-S0/E clusters having a steeper elliptical distribution.

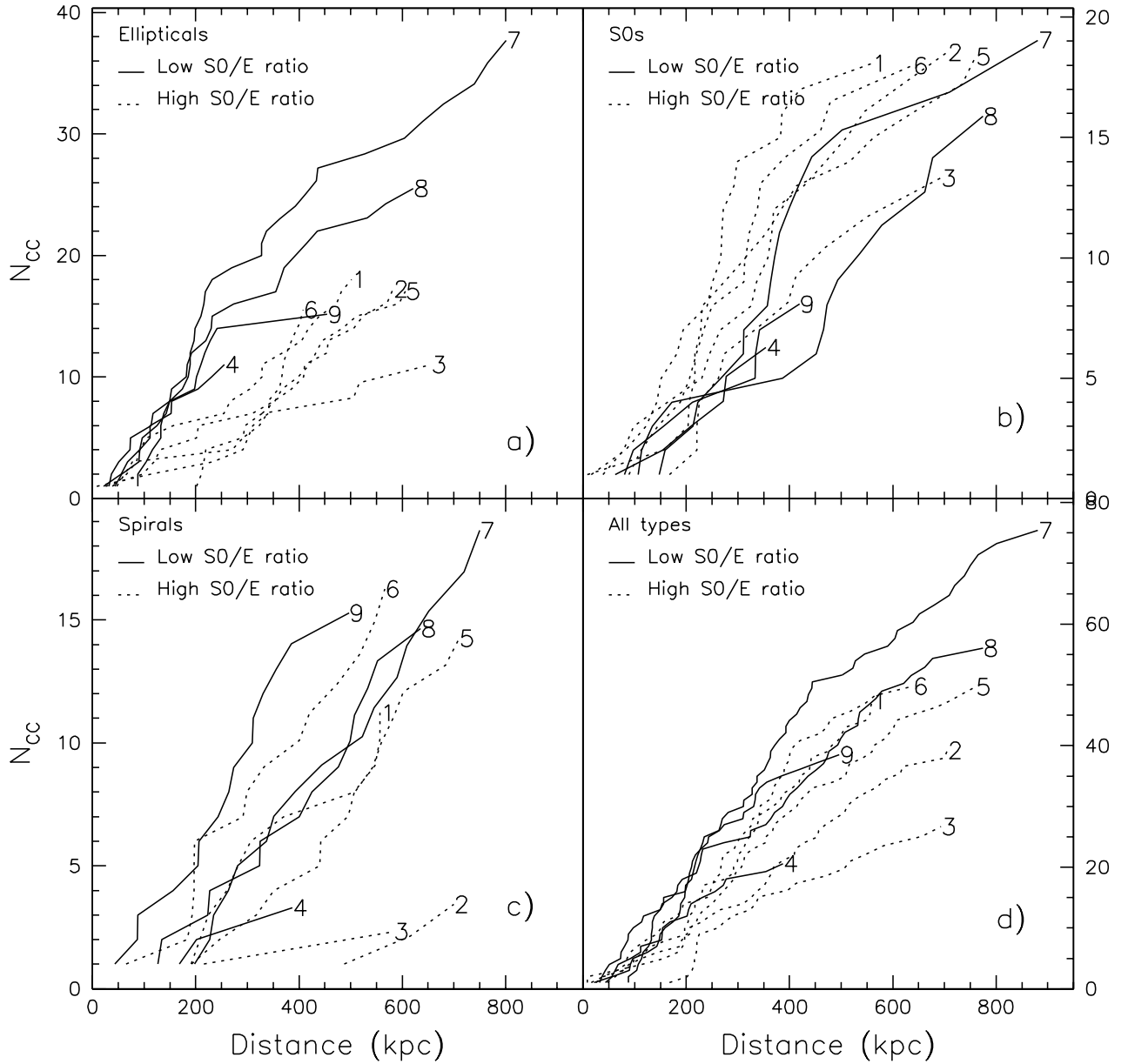


Fig. 7. Cumulative but un-normalized radial distributions of individual low-S0/E and high-S0/E clusters (full and dotted lines, respectively), corrected for area incompleteness as explained in the text.

In the following, the clusters with a high and low concentration of ellipticals will be indicated by the acronyms *HEC* and *LEC*. It is worth noting that, since in our sample there is a perfect correspondence between the concentration of ellipticals and S0/E ratio, our *HEC* and *LCE* clusters coincide with the low-S0/E and high-S0/E sub-sets, respectively.

4.1. Evolution in morphological content

We will now investigate the evolution of the galactic morphologies by comparing our results with other studies at lower and higher redshift.

Before performing this comparison, we have applied 3 different statistical corrections to our raw counts in Table 4: (i) The correction for incompleteness due to the irregular shape of the area surveyed was computed according to the procedure outlined in the previous section (see caption of Fig.7). (ii) The systematic differences in the morphological classifications between WJC+MORPHS and GF (see §3), were corrected for by making the appropriate adjustments to GF’s morphological counts. Specifically, we have multiplied GF’s S0 counts by 73/57 and, in order to preserve the total counts, we have taken the differential counts from both the E and Sp populations according to the relative percentages given in section 3 (75% and 25% , respectively). (iii) The field contamination was determined from the galaxy number counts given by Metcalfe et al. (1995) and the breakdown into morphological classes (E/S0/Sp=18:27:56) was computed for our limiting magnitudes at $z \sim 0.2$ from the fits to the differential number counts of the Medium Deep Survey (S97). The background assumed is listed for each cluster in Table 5 which is available in CD-ROM form. The number of contaminating early-type galaxies was found to agree with the number of probable background galaxies redder than the elliptical sequence in the color-magnitude plots, hence local background variations should not be dramatic towards the clusters in this sample. As it will be clear in the following discussion, the uncertainty introduced by the field contamination has negligible consequences on our results.

At higher redshifts, we consider the MORPHS distant cluster sample plus five additional clusters in the range $z = 0.2 - 0.3$. The latter include the 3 clusters at $z \sim 0.3$ from the *HST*-based morphological study of Couch et al. (1998), together with A2218 and A1689 (both at $z = 0.18$) for which archival HST/WFPC-2 images were available. These images were used by WJC to morphologically classify the galaxies in A2218 and A1689, in the same way as was done for the Couch et al. and MORPHS studies. Details of all 5 clusters are given in Table 6; hereafter we shall refer to them as the C98+ sample.

As for our clusters, the morphological number counts of the MORPHS and the C98+ samples have been computed down to $M_V = -20$ and the raw counts have been corrected for incompleteness due to the irregular shape of the area surveyed, (according to the procedure outlined earlier) and for field contamination. The latter were determined from the morphological galaxy number counts of the Medium Deep Survey as in S97. The magnitude limits adopted for the C98+ clusters are listed in Table 6. The limits for the MORPHS dataset are $M_{lim}^{D97} - 1$ mag, where M_{lim}^{D97} is given in Table 1 of D97.³ The magnitude limits were derived adopting the transformations between the *HST* and standard photometric bands given by Holtzman et al. (1995). The Cousins *I*-band calibration of the HST A1689 image was kindly provided by I. Smail.

³In fact, due to a transcription error in D97, M_{lim}^{D97} corresponds to $M_V = -19$.

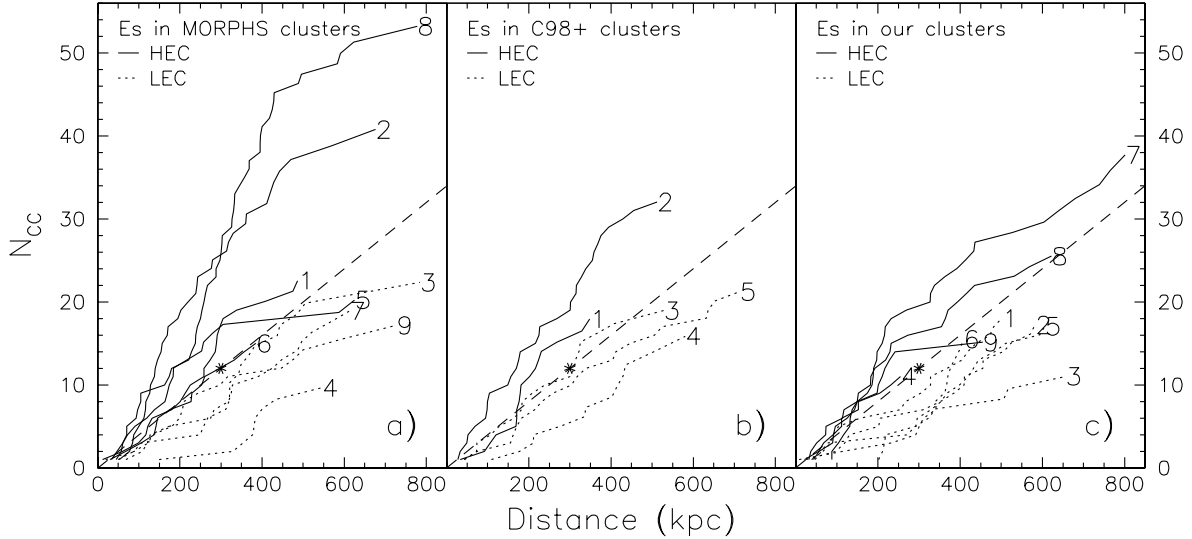


Fig. 8. Corrected cumulative distributions of ellipticals in the MORPHS and C98+ clusters (panel a and b, respectively), compared with the corresponding distributions from our lower redshift sample (panel c). Full and dotted lines represent clusters above and below the arbitrary cut-off point $R = 300$ kpc, $N_{CC}=12$ (asterisk). The numbers at the end of each line identify the clusters according to the ranking order in Table 4 (our sample), in Table 6 (C98+ sample) and according to the following order for the MORPHS sample: 1) Cl1447; 2) Cl0024; 3) Cl0939; 4) Cl0303; 5) 3C295; 6) Cl0412; 7) Cl1601; 8) Cl0016; 9) Cl0054.

To discuss the distant cluster data in the framework of the previously noted S0/E dichotomy, we have also tried to classify the MORPHS and the C98+ clusters according to our bimodal scheme *HEC/LEC*. In Figure 8, the corrected cumulative counts (N_{CC}) of the elliptical galaxies in the MORPHS and C98+ samples (Fig. 8a,b) are compared with the distributions in our sample (Fig. 8c; see also Fig. 7a). Even if no clear separation between *HEC* and *LEC* exists among the clusters in Figures 8a and 8b, we have tentatively divided both samples according to the arbitrary criterion (also working in Fig. 8c for our sample) that clusters having $N_{CC}(R = 300 \text{ kpc}) > 12$ (< 12) belong to the *HEC* (*LEC*) family (see asterisks and dashed lines in Fig. 8).

TABLE 6: C98+ SAMPLE

| Cluster | z | Area(Mpc^2) | Ref. | M_{lim} |
|----------|-------|------------------------|------|---------------------|
| 1) A2218 | 0.171 | 0.4 | WJC | 19.48 F702W (HST R) |
| 2) A1689 | 0.181 | 1.0 | WJC | 19.17 I |
| 3) AC118 | 0.308 | 0.6 | C98 | 20.80 F702W (HST R) |
| 4) AC103 | 0.311 | 0.6 | C98 | 20.80 F702W (HST R) |
| 5) AC114 | 0.312 | 1.0 | C98 | 20.80 F702W (HST R) |

At low redshift, we refer to D80a and Oemler (1974; hereafter O74) as local benchmarks. The morphological fractions and ratios of the high- and low-concentration nearby clusters (with a 1 Mpc^2 area cut) of D80a were obtained from Table 2 and Fig. 3 in D97. In the following figures we also plot the values quoted by Oemler (1974, O74) for different cluster types. Oemler divided clusters at low redshift into three groups: spiral-rich (SR), elliptical-rich (ER) and S0-rich (S0R, named spiral-poor by O74) according to their galaxy content (ER: E:S0:Sp=3:4:2; SR: E:S0:Sp=1:2:3; S0R: E:S0:Sp=1:2:1). We will come back to this point in §6; here we want to stress that Oemler’s low redshift points should be considered only as indicative because they were not found applying the same magnitude and area limits used in this work and have been taken from the approximate ratios given by O74. Moreover, it is also worth stressing that the correspondence between the D80a high(low)-concentration clusters and our *HEC(LEC)* clusters is far from being demonstrated.

The fully-corrected morphological fractions and ratios of all the clusters as a function of redshift are presented in Figs. 9 and 10, highlighting the *HEC/LEC* dichotomy (filled/open symbols represent *HEC/LEC* clusters respectively). In order to evaluate the errors associated with background subtraction, we have computed the changes in the morphological fractions that occur if the field correction for each cluster and galactic type is varied by an amount equal to the correction itself (100% error, see Table 5 available in CD-ROM form). The variation in the morphological fractions is on average 0.03, ranging between 0.01 and 0.08. In Figs. 9 and 10 the errorbars represent the Poissonian errors due to the small numbers of galaxies and are typically greater than 0.1. Therefore the Poissonian errors always dominate over the errors due to field subtraction.

In spite of the large errors, it is clear from these figures that there are systematic trends with z : the spiral fraction declines and the S0 fraction rises in going towards lower redshifts. The morphological fractions in our clusters are intermediate between the high and the low redshift values and seem to trace a continuous change of the abundance of S0 and spiral galaxies. In contrast, the elliptical fraction (top panel in Fig. 9) shows no particular trend with redshift, but rather a large scatter from cluster to cluster at any epoch. The mirror-like trends of the S0 and spiral fractions (Figures 9b,c) are well represented by the behaviour of the S0/Sp ratio in Fig. 10b. From this, we can confidently argue that, as the redshift becomes lower, the S0 population tends to grow at the expense of the spiral population.⁴

Figure 10a suggests the existence of a large intrinsic scatter in the S0/E ratio, which, at least within our sample, can be mostly ascribed to the different cluster morphologies: clusters showing a marked concentration of ellipticals in the central region have lower S0/E ratios with respect to the clusters in which E galaxies are more or less uniformly distributed inside the cluster area. A similar tendency is possibly seen at higher redshift as well and at low redshift comparing elliptical-rich and S0-rich clusters. The dotted and dashed straight lines in Figure 10a represent the formal least-square weighted fits ($0.09 < z < 0.65$) to the HEC and LEC clusters, respectively. In spite of the scatter, likely due to the intrinsic dependency of the S0/E ratio on the cluster morphology, the trend with redshift found by D97 (full line in Figure 10a) turns out to be confirmed.

⁴While this paper was being refereed, a morphological study of the cluster CL1358+62 at $z=0.33$ appeared as a preprint (Fabricant, Franx & van Dokkum 2000). The area covered in this study is bigger than the area considered here; nevertheless, the morphological fractions – as independently classified by the authors and by A. Dressler – fall in both cases within the typical values observed at that redshift in Fig. 9.

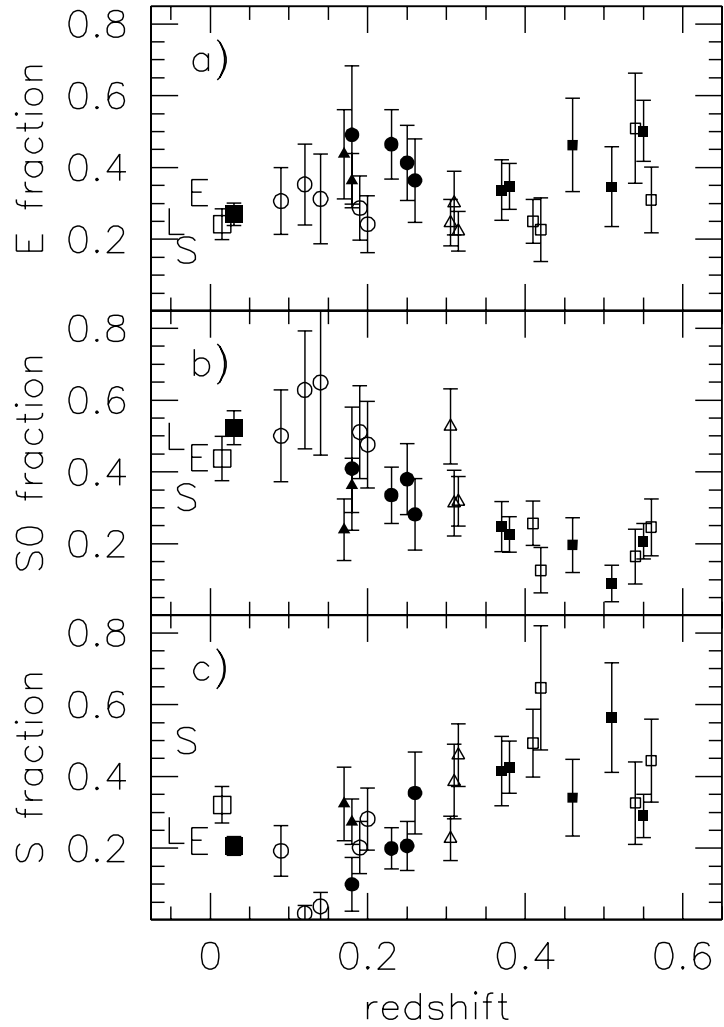


Fig. 9. Morphological fractions as a function of redshift. *HEC* and *LEC* clusters are displayed as solid and open symbols, respectively. The values from our sample are indicated by circles, whereas those from the MORPHS and C98+ samples are indicated with squares and triangles, respectively. All these data are corrected both for field contamination and for the irregular shape of the area surveyed (see text). The errorbars correspond to Poissonian values. The average values derived for high- (*large solid squares*) and low-concentration (*large open squares*) clusters from D80 (see text) are plotted at $z \sim 0$. Oemler's datapoints are indicated with letters (E = elliptical-rich; L = S0-rich; S = spiral-rich) and are placed at $z < 0$ for display purposes.

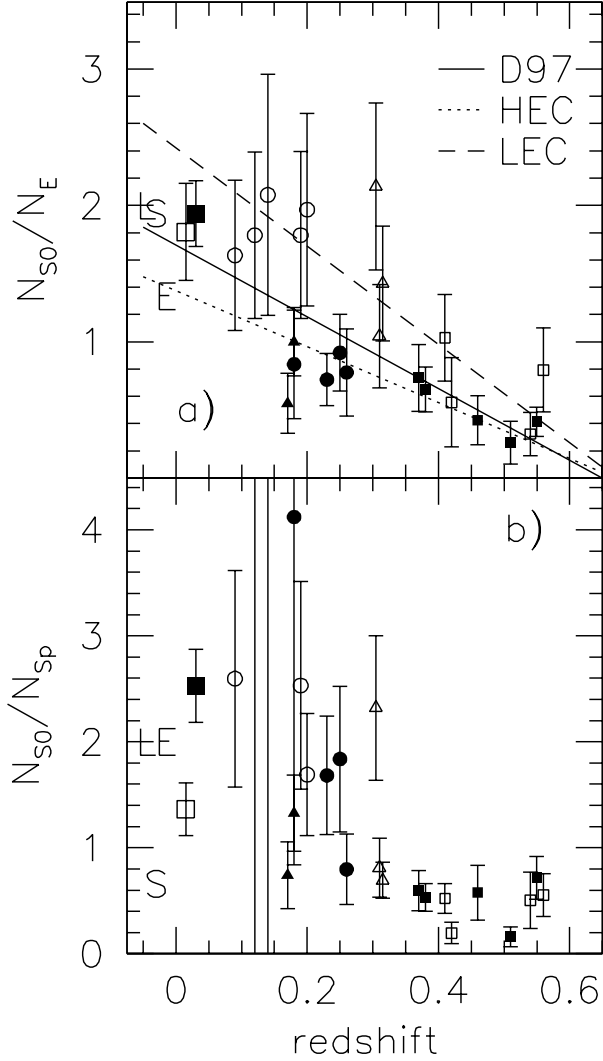


Fig. 10. The S0/E and S0/Sp ratios as a function of redshift. The meaning of the symbols is as in Fig. 9. The dotted and dashed lines in the top panel represent the least square weighted fits ($0.09 < z < 0.65$) to the HEC and LEC clusters, respectively. The linear regression of the MORPHS data given by D97 is represented by the *solid* line.

5. The morphology-density relation

In this section we examine the relative occurrence of each morphological type as a function of the local projected density of galaxies (i.e. the morphology-density relation). The local densities have been computed

– following D80a and D97 – in a rectangular area containing the 10 nearest neighbors. In Figure 11 we present the local density distributions of galaxies of the different morphological types (upper panels), together with the corresponding distributions of morphological fractions (lower panels) for our global cluster sample (leftmost panels), as well as the *LEC* and *HEC* sub-samples (middle and rightmost panels).

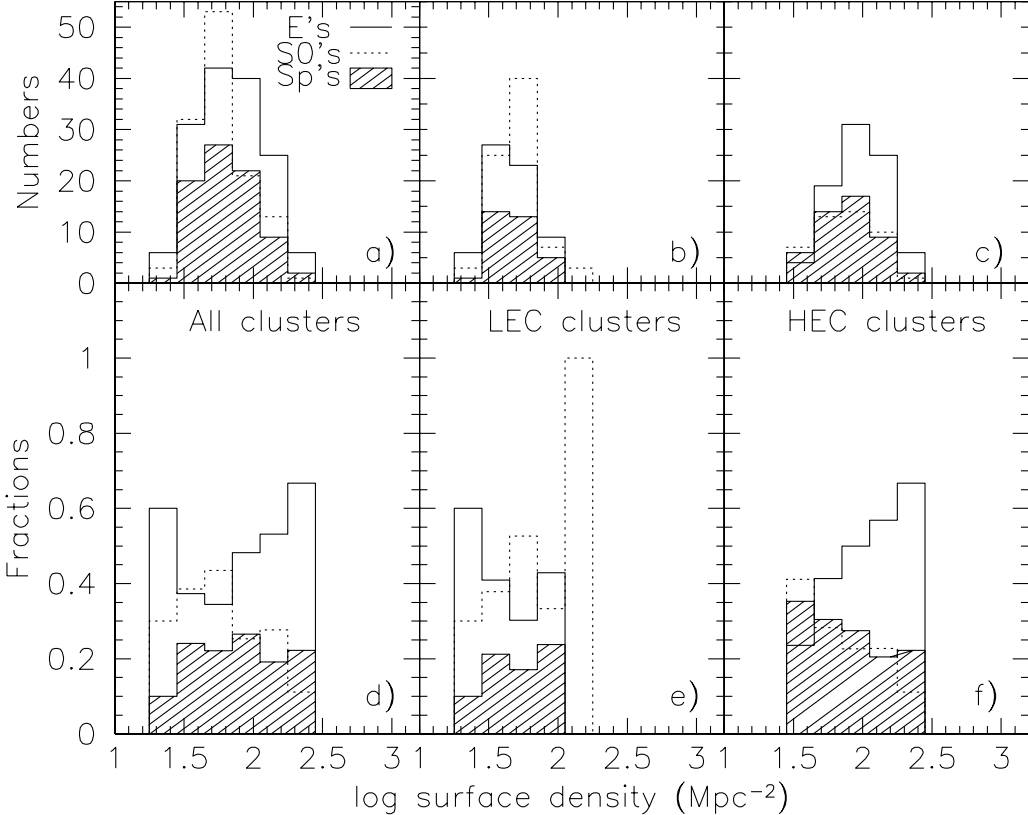


Fig. 11. Number and fraction of galaxies of different morphological types as a function of the local density for the 9 clusters in our sample (leftmost panels) and for the sub-samples of *LEC* (middle panels) and *HEC* (rightmost panels) clusters. The distributions of elliptical, S0 and spiral galaxies are indicated with a full line, a dotted line and a shaded histogram, respectively.

Apart from the different value of the global S0/Sp ratios, our distributions (Fig. 11d, e and f) look qualitatively very similar to those of the MORPHS sample (Figs. 4, 5 and 6 in D97), particularly if we compare our *HEC* and *LEC* cluster families with the high- and low-concentration families in D97. As in the higher redshift clusters, a morphology-density relation is present in highly concentrated clusters and absent in the low concentration clusters where a possible small *anticorrelation* can be noted both here and in D97. The fact that the density distributions at $z \sim 0.1$ resemble those at $z \sim 0.5$ much more closely than those at $z \sim 0$ could suggest that the morphology-density relation in low concentration clusters was established in the last 1-2 Gyr, but a definite conclusion cannot be reached on the basis of the available data.

Another remarkable feature of the MD distributions is that, moving from high redshift to the intermediate redshift regime, the fraction of Es as a function of the local density appears to be practically unchanged for both *HEC* and *LEC* clusters, i.e. the elliptical-density relations at $z = 0.2$ are also *quantitatively* similar to that of the MORPHS sample at $z = 0.5$. We also note that the *LEC* distributions remain relatively flat over this redshift interval, while a strong increase in the S0/Sp fraction takes place (compare our Fig. 12e with Fig. 8 in D97). This suggests that in the *LEC* clusters the Sp \rightarrow S0 transformation process is highly efficient and that the efficiency is largely independent of local density. In contrast, the S0- and spiral-density distributions in *HEC* clusters at the two different redshifts (compare our Fig. 11f with Fig. 6 in D97), have quite different slopes, suggesting that the process of transfer from spirals to S0s is more efficient in low density regions than in high density ones. The above analysis is based on the comparison of two rather small cluster samples and, therefore, it needs to be confirmed by the morphological study of more sizeable samples. Nevertheless, there is the suggestion that, at least in our range of observed local densities ($1.3 \lesssim \log \rho \lesssim 2.4$), the efficiency of the possible transition from spiral to S0 morphology seems to increase with decreasing local density.

Finally, the fact that no MD relation is found in our *LEC* clusters demonstrates that the dichotomy in the S0/E ratio discussed in the previous section cannot merely be ascribed to a universal MD relation at $z = 0.2$ combined with different density ranges for the *HEC* and *LEC* clusters: the two types of clusters are intrinsically different both in their global morphological content and in the arrangement of the morphological types as a function of the local density.

6. Conclusions

1) The morphological properties of the galaxy populations in nine clusters at $z = 0.1 - 0.25$ are found to be intermediate between those at $z \sim 0.4 - 0.5$ and those at low- z , with a moderate spiral content and a moderate “deficiency” (as compared to lower redshifts) of S0 galaxies. Our results support the evolutionary scenario, inferred from higher redshift studies (D97, S97, Couch et al. 1998), involving the disk galaxy populations in which there is a progressive morphological conversion in clusters, from spirals into S0’s.

2) At $z \sim 0.2$, we find a dichotomy in the relative occurrence of S0 and elliptical galaxies: four of our clusters display a low S0/E ratio (~ 0.8) while two of our clusters have a significantly higher ratio (~ 1.9) similar to the other clusters in our sample at $z = 0.1$. The most likely interpretation of this dichotomy and of the large scatter in the S0/E ratio at $z \sim 0.2$ is that such a ratio is both a function of the redshift and of the cluster “type”, being significantly lower in clusters with a strong central concentration of elliptical galaxies.

3) At $z \sim 0.1 - 0.2$ a morphology-density relation exists only for the high-concentration clusters and is absent in the low-concentration ones. The same result was found at $z \sim 0.5$ (D97), while at low redshift the correlation between galaxy morphology and local density is present in all types of clusters of the D80a sample. Although the number of galaxies is too small to draw definite conclusions, these results seem to suggest that the morphology-density relation in low-concentration clusters was established only in the last 1-2 Gyr, but only additional data and a homogeneous systematic analysis both at low and moderate redshifts will clarify this matter. Moreover, comparing our MD relations with the corresponding ones at $z \sim 0.5$ (D97), we suggest that the efficiency of the Sp \rightarrow S0 transformation process anticorrelates with the local density.

The relation between the S0/E ratio and the spatial concentration of the ellipticals is not surprising in the light of the well-known correlations between the galaxy content and the cluster type in low-redshift clusters. As mentioned in §4, Oemler (1974) grouped clusters in three classes: spiral-rich (SR), elliptical-rich (ER, the most spherical in shape and concentrated) and S0-rich (S0R, named “spiral-poor” by O74, “not quite as centrally concentrated as the ER class, but more regular than the SR class”). Interestingly, O74 suggested that S0-rich clusters are dynamically evolved clusters (they already show segregation by mass and morphological type) representing a later evolutionary stage of spiral-rich clusters, following the evolution of a significant fraction of the spiral galaxies into S0’s. In contrast, in the scenario proposed by O74, E-rich clusters are well evolved but *intrinsically different* from the S0R clusters: although possibly the dynamically oldest type of clusters, their high elliptical content implies that they did not evolve from the spiral-rich clusters and is likely due to an enhanced formation rate of ellipticals in regions that began as the densest fluctuations in the early universe.

We speculate that in our sample at $z \sim 0.2$, the four clusters with a strong central concentration of ellipticals (and the lowest S0/E ratios) are presumably the analogues (and progenitors) of the low- z E-rich clusters (see the extrapolation at low redshift of dotted line in Figure 10a), while the low-concentration clusters (with the highest S0/E ratio) seem to be the analogues of the “S0-rich” clusters.

The effects of redshift (evolution) and cluster type are expected to mingle in various proportions at the different epochs. Following O74, we suggest that the relative occurrence of S0’s and spirals is mostly linked with the “maturity” of the cluster with spirals progressively evolving into S0’s, while the ellipticals are well in place at redshifts greater than those considered here and their abundance and concentration reflect an “original imprinting” (see also D97). Then, the S0/Sp ratio should be related to the evolutionary epoch of the cluster and the S0/E value should be determined both by the epoch and the cluster type (nurture and nature, in a way), with the redshift being the dominant effect at early epochs.⁵

Acknowledgements

Based on observations made with the Nordic Optical Telescope, La Palma, and the Danish 1.5-m telescope at ESO, La Silla, Chile. The Nordic Optical Telescope is operated jointly by Denmark, Finland, Iceland, Norway, and Sweden, in the Spanish Observatorio del Roque de los Muchachos of the Instituto de Astrofísica de Canarias.

The authors are grateful to the anonymous referee for the prompt refereeing that helped us to improve the rigor and clarity of this paper. BMP and WJC warmly thank Ian Smail for providing the images and the photometric catalog of A1689, for his valuable assistance in this project, for carefully reading the manuscript and suggesting a number of changes that improved the paper. They are also thankful to their colleagues of the MORPHS group for many interesting discussions and useful advice.

⁵If the ER and S0R clusters are the endpoints of the evolution of two originally-different types of clusters and both types experienced the accretion of large numbers of spirals that with time turned into S0’s, then when looking further back in time, the difference in the S0/E ratio between the precursors of the ER and of the S0R clusters should become smaller and smaller: at $z \sim 0.4 - 0.5$ all types of clusters are expected to display a low S0/E ratio (with smaller fluctuations among the different types of clusters), as indeed is observed in the MORPHS dataset, simply because many of the S0’s have not yet formed.

This work was supported by the Formation and Evolution of Galaxies network set up by the European Commission under contract ERB FMRX-CT96-086 of its TMR program and by the Danish Natural Science Research Council through its Centre for Ground-Based Observational Astronomy. WJC acknowledges the Schools of Physics at Bristol and St Andrews Universities and the European Southern Observatory for their hospitality during the course of this work. This research has made use of the NASA/IPAC Extragalactic Database (NED) which is operated by the Jet Propulsion Laboratory, Caltech, under contract with the National Aeronautics and Space Administration.

REFERENCES

Abadi, M. G., Moore, B., Bower, R. G., 1999, MNRAS, 308, 947
Andreton, S., Davoust, E., Heim, T., 1997, A&A, 323, 337
Andreton, S., 1998, ApJ, 501, 533
Barger, A. J., Aragón-Salamanca, A., Smail, I., Ellis, R. S., Couch, W. J., Dressler, A., Oemler, A. Jr., Poggianti, B. M., Sharples, R. M., 1998, ApJ, 501, 522
Bautz, L.P., Morgan, W.W., 1970, ApJ, 162, L149
Bertin, A., Arnouts, S., 1996, A&AS, 117, 393
Butcher, H., Oemler, A. Jr., 1978, ApJ, 226, 559
Butcher, H., Oemler, A. Jr., 1984, ApJ, 285, 426
Capaccioli, M., Vietri, M., Held, E.V., Lorenz, H., 1991, ApJ, 371, 535
Couch, W. J., Barger, A. J., Smail, I., Ellis, R. S., Sharples, R. M., 1998, ApJ, 497, 188
Couch, W. J., Ellis, R. S., Sharples, R. M., Smail, I., 1994, ApJ, 430, 121
Dressler, A., 1980a, ApJ, 236, 351 (D80)
Dressler, A., 1980b, ApJS, 424, 565 (DCAT80)
Dressler, A., Oemler, A. Jr., Butcher, H., Gunn, J. E., 1994, ApJ, 430, 107
Dressler, A., Oemler, A. Jr., Couch, W. J., Smail, I., Ellis, R. S., Barger, A., Butcher, H., Poggianti, B. M., Sharples, R. M., 1997, ApJ, 490, 577 (D97)
Dressler, A., Smail, I., Poggianti, B. M., Butcher, H., Couch, W. J., Ellis, R. S., Oemler, A. Jr., 1999, ApJS, 122, 51
Ebeling, H., Edge, A., Bohringer, H., Allen, S., Crawford, C., Fabian, A., Voges, W., Huchra, J., 1998, MNRAS, 301, 881
Ellis, R. S., Smail, I., Dressler, A., Couch, W. J., Oemler, A. Jr., Butcher, H., Sharples, R. M., 1997, ApJ, 483, 582
Fabricant, D., Franx, M., van Dokkum, P., 2000, ApJ, in press (astro-ph 0003360)
Fasano, G., Bettoni, D., D'Onofrio, M., Kjærgaard, P., Moles, M., 2000, in preparation
Fasano, G., Vio, R., 1991, MNRAS, 249, 629
Franceschini, A., Silva, L., Fasano, G., Granato, G.L., Bressan, A., Arnouts, S., Danese, L., 1998, ApJ, 506, 600
Frei, Z., Guhathakurta, P., Gunn, J. E., Tyson, J. A., 1996, AJ, 111, 174
Holtzman, J. A., Burrows, C. J., Casertano, S., Hester, J. J., Trauger, J. T., Watson, A. M., Worthey, G., 1995, PASP, 107, 1065
Jones, C., Forman, W., 1999, ApJ, 511, 65
Jorgensen, I., 1994, PASP, 106, 967
Kelson, D. D., van Dokkum, P. G., Franx, M., Illingworth, G. D., Fabricant, D., 1997, ApJ, 478, L13
Kelson, D. D., Illingworth, G. D., van Dokkum, P. G., Franx, M., 1999, ApJ, in press (astro-ph 9906152)
Landolt, A.U., 1992, AJ, 104, 340
Lavery, R. J., Henry, J. P., 1988, ApJ, 330, 596

Lavery, R. J., Pierce, M. J., McClure, R. D., 1992, AJ, 104, 2067

Lavery, R. J., Henry, J. P., 1994, ApJ, 426, 524

Lubin, L. M., Postman, M., Oke, J. B., Ratnatunga, K.U., Gunn, J. E., Hoessel, J. G., Schneider, D. P., 1998, ApJ, 116, 584

Mathis, J. S., 1990, ARAA, 28, 37

Metcalfe, N., Shanks, T., Fong, R., Roche, N., 1995, MNRAS, 273, 257

Moore, B., Katz, N., Lake, G., Dressler, A., Oemler, A. Jr. 1996, Nature, 379, 613

Moore, B., Lake, G., Katz, N., 1998, ApJ, 495, 139

Oemler, A. Jr., 1974, ApJ, 194, 1

Oemler, A. Jr., Dressler, A., Butcher, H., 1997, ApJ, 474, 561

Poggianti, B. M., 1997, A&AS, 122, 399

Poggianti, B. M., Smail, I., Dressler, A., Couch, W. J., Barger, A. J., Butcher, H., Ellis, R. S., Oemler, A. Jr., 1999, ApJ, 518, 576

Pignatelli, E., Fasano, G., 1999, Proceedings: *First Italian Workshop of the "Network sulla formazione ed evoluzione delle galassie"*, <http://www.brera.mi.astro.it/docB/galaxy/news.html>

Rood, H.J., Sastry, G.N., 1971, PASP, 83, 313

Simien, F., de Vaucouleurs, G., 1986, ApJ, 302, 564

Smail, I., Dressler, A., Couch, W. J., Ellis, R. S., Oemler, A. Jr, Butcher, H., Sharples, R. M., 1997, ApJS, 110, 213 (S97)

Smail, I., Edge, A. C., Ellis, R. E., Blandford, R. D., 1998, MNRAS, 293 124

Thompson, L. A., 1986, ApJ, 300, 639

Thompson, L. A., 1988, ApJ, 324, 112

van Dokkum, P. G., Franx, M., 1996, MNRAS, 281, 985

van Dokkum, P. G., Franx, M., Kelson, D. D., Illingworth, G. D., Fisher, D., Fabricant, D., 1998, ApJ, 500, 714

van Dokkum, P.G., Franx, M., Fabricant, D., Kelson, D. D., Illingworth, G. D., 1999, ApJ, 520, L95

van Dokkum, P.G., Franx, M., Fabricant, D., Illingworth, G. D., Kelson, D. D., 2000, ApJ, in press (astro-ph 0002507)

Wirth, G. D., Koo, D. C., Kron, R. G., 1994, ApJ, 435, L105